Zero-thickness interface constitutive theory for concrete self-healing effects

Antonio Caggiano [a, b, *], Guillermo Etse [a, b, c], Liberato Ferrara [d], Visar Krelani [d]

[a] *Consejo Nacional de Investigaciones Cientificas y Tecnicas (CONICET), Argentina*
[b] *Universidad de Buenos Aires, Facultad de Ingeniera, INTECIN - CONICET, Argentina*
[c] *Universidad Nacional de Tucuman, Facultad Ciencias Exactas y Tecnologia, Argentina*
[d] *Department of Civil and Environmental Engineering, Politecnicno di Milano, Italy*

ABSTRACT

A damage-plasticity constitutive theory for zero-thickness interfaces is presented aimed at predicting time-dependent self-healing phenomena in concrete. The material model is based on fracture-energy concepts and accounts for the time evolution of concrete porosity induced by the self-healing mechanism. The accuracy and soundness of the proposed interface model are demonstrated through comparative analyses of model predictions against experimental results on three point beam tests performed up to crack opening and then, up to complete failure, before and after been subjected to different exposure conditions, respectively. A wide range of experimental tests was considered in this work for both calibration and validation purposes of the proposed interface model.

© 2016 Published by Elsevier Ltd.

1. Introduction

Concrete is the most widely used construction material in the world. Global cement production contributes to about 5% of annual greenhouse gas emissions (a level quite similar to those of the aviation sector), and the CO_2 released into the atmosphere, significantly affects Earth's temperature while contributes to the global warming [1]. Thus, there is an increasing demand of adopting eco-friendly design solutions in civil and structural engineering [2]. In this framework, the availability of self-healing cement-based materials capable to prevent the permeation of chemically aggressive agents, thus improving the structure durability, represents an important contribution to the achievement of eco-sustainable and greener structures [3,4].

Nowadays, there is a consensus in the international scientific community regarding the significance and benefits of concrete self-healing features. This is based on numerous studies and contributions which allowed gaining a more clear understanding of the involved phenomena. Important conclusions of the progress made in this field are summarized in RILEM TC-221-SHC which establishes that the self-healing phenomenon in cement-based materials involves two different mechanisms: (i) the "self-closing" and (ii) the "self-healing", respectively. The first one indicates only the closure of cracks, while the second one deals with the restoring of the mechanical properties due to healing processes. RILEM TC-221-SHC also defines the difference between "autogenic" (natural) and "autonomic" (engineered) self-clos-

ing/healing, depending on whether the crack closure or restoration of material properties is due to either the concrete material itself or triggered by means of engineered additions [5].

In the last decades, several researches and studies were aimed at investigating the physical/chemical/mechanical behavior of cementitious materials containing "engineered" self-healing components. In this field, the use of Crystalline Additives (CAs) has been successfully explored by Sisomphon et al. [6], and Ferrara et al. [7]. These studies have shown that CAs strongly boost the mechanical restoration due to the surface crack closing phenomena while it reduces the leakage of water through cracks. Wiktor and Jonkers [8] have demonstrated and quantified the crack-healing potential of a specific two-component bio-chemical self-healing agent, embedded in clay particles which serve as particles reservoir, and partially replace the regular concrete aggregates. The capability of developing self-healing mechanism by employing polyurethane material, encapsulated by glass or ceramic cylindrical capsules to seal cracks, was shown [9]. State of the start reviews on self-healing phenomena in cement-based materials are published in the references [10–12].

Regarding constitutive theories and modeling of self-healing mechanism and its effect on the overall mechanical response behavior of concrete, all of the available proposals in the literature follow the so-called smeared-crack approach. In this sense, few constitutive models were developed so far for predicting the delayed hydration in cementitious materials and/or the carbonation process which take place due to self-healing, see [13]. Some proposals like He et al. [14] determine the amount of unhydrated cement particles in concrete specimens as a function of the water-to-cement ratio and the cement fineness which are input parameters. Recently, a constitutive model was formulated by Huang and Ye [15] aimed at simulating the hydration process in

* Corresponding author at: Consejo Nacional de Investigaciones Cientificas y Tecnicas (CONICET), Argentina.
Email addresses: acaggiano@fi.uba.ar (A. Caggiano); getse@herrera.unt.edu.ar (G. Etse); liberato.ferrara@polimi.it (L. Ferrara); visar.krelani@polimi.it (V. Krelani)

concrete using water transport and ion diffusion theories as well as thermodynamics laws. However, these models do not provide any information about the mechanical effects of self-healing. An interesting proposal is due to Lv and Chen [16] who consider a generalized reaction approach to model the hydration of cement particles. Thereby, the self-healing efficiency is quantitatively taken into account in terms of the volume fraction, the particle size distribution and the cracking modes of unhydrated cement nuclei. A coupled hydro-chemo-mechanical model is proposed in [17] to simulate the autogenous healing phenomenon of high performance concrete. Di Luzio and Cusatis [18] have formulated a Solidification-Microprestress-Microplane (SMM) model which predicts the self-healing mechanism through a suitably internal variable accounting for the cracking effects on both diffusion phenomena and also for the recovering effect due to crack-healing process [19].

This work reports the development of a zero-thickness interface model conceived in the framework of a coupled damage-plastic theory. Main objective of this proposal is the modeling of concrete cracking and failure behavior under the consideration of self-healing processes. The interface model is formulated within the general framework of the flow theory of plasticity and the continuum damage theory. The post-peak response is controlled by fully independent fracture energy-based mechanisms for both mode I and II types of failure. Based on a previous proposal by the first and second authors [20], the interface constitutive model is now extended to account for the self-healing effects on concrete stiffness, strength and post-peak response behavior under all possible fracture modes. For this purpose a self-healing porosity parameter is formulated which governs the variation of concrete main mechanical features such as strength and stiffness through the softening and damage rule descriptions.

It is worth mentioning that classical or local strain softening models, based on the Smeared Crack Approach (SCA), lead to strong loss of objectivity regarding mesh size and orientation due to the loss of ellipticity of the involved differential equations, see also [21,22]. Thus, regularization strategies are required to suppress the ill-possessedness of the differential equations [23,24] which, at the same time, lead to unrealistic redistribution and diffusion of the failure patterns. That it is why, Discrete Crack Approaches (DCAs) have became progressively attractive in solid failure mechanics. The interface model for concrete failure behavior under self-healing effects in this proposal follows the discrete crack approach and, therefore, is related to objective failure predictions regarding mesh size and orientation.

DCAs may be classified in direct ones and "on-the-fly" types. Interface model approaches [25,26] as the one in this proposal, but also the lattice models [27,28] and the particle model schemes [29,30] belong to the direct procedure. Others, such as the E-FEM [31,32], X-FEM [33,34] and the Element-Free-Galerkin [35,36] methods belong to the on-the-fly type of DCAs, as they introduce crack discontinuities within continuous FE domains during monotonic loading processes, once certain conditions (i.e., discontinuous bifurcation) are fulfilled. These conditions may also define the direction of the discontinuity.

After this introductory section, the proposed damage/plasticity interface model for simulating concrete failure and post-cracking processes before and after self-healing phenomena, respectively, is formulated. The descriptions of the strength and stiffness degradation mechanisms of the interface model in the framework of the flow theory of plasticity and the isotropic damage theory are proposed in Sections 3 and 4, respectively. The experimental results considered for the model calibration are reported in Section 5. The experimental campaign deals with the analysis of concrete with and without crystalline admixtures. The self-healing has been assessed by investigating

the recovery of concrete mechanical properties, as determined by means of three-point bending tests performed to precrack the specimens. Then, once the specimens were exposed to different environments (water immersion and air exposure), the three-point bending tests were continued up to failure. Test data are employed as benchmark to validate the proposed interface model. Comparisons between experimental data and numerical predictions are presented and discussed in Section 6. Finally, Section 7 remarks the key results of the present research and highlights possible future research steps.

2. Coupled damage-plasticity interface model

Applying the Prandtl-Reuss additive decomposition law to the interface kinematic field,

$$\dot{\mathbf{u}} = \dot{\mathbf{u}}^{el} + \dot{\mathbf{u}}^{cr}, \tag{1}$$

with

$$\dot{\mathbf{u}}^{el} = \mathbf{C_d}^{-1} \cdot \dot{\mathbf{t}} \tag{2}$$

The coupled damage-elastoplastic constitutive equation of the interface can be expressed as

$$\dot{\mathbf{t}} = \mathbf{C_d} \cdot (\dot{\mathbf{u}} - \dot{\mathbf{u}}^{cr}) \tag{3}$$

thereby $\dot{\mathbf{u}} = [\dot{u}, \dot{v}]^t$ is the vector of relative velocities across the interface, $\dot{\mathbf{u}}^{el}$ and $\dot{\mathbf{u}}^{cr}$ are the elastic and cracking (inelastic) velocity vector components, respectively, $\dot{\mathbf{t}} = [\dot{\sigma}_N, \dot{\sigma}_T]^t$ is the interface stress rate vector and $\mathbf{C}_d$ the elastic-damage stiffness matrix

$$\mathbf{C_d} = (\mathbf{I} - \mathbf{D}) \cdot \mathbf{C} \tag{4}$$

being $\mathbf{I}$ the second order identity matrix and $\mathbf{C}$ the undamaged elastic matrix.

Provided the concept "effective interface stress" is considered [37], the plastic response can be integrated independently of the damage mechanics one. Under this hypothesis Eq. (3) can be reformulated as

$$\begin{aligned} \dot{\mathbf{t}} &= (\mathbf{I} - \mathbf{D}) \cdot \tilde{\mathbf{t}} \\ \dot{\tilde{\mathbf{t}}} &= \mathbf{C} \cdot \dot{\mathbf{u}}^{el} \end{aligned} \tag{5}$$

being $\tilde{\mathbf{t}}$ the rate of the effective interface stress vector. Moreover, the plastic interface velocities can be computed in the effective stress space, thus independently of the damage corrector which is separately evaluated.

The tangential material operator can be finally obtained in three numerical steps:

- evaluate the elastic predictor,
- calculate the plastic corrector and
- obtain the damage corrector.

The expression of the tangential elastic-damage-plastic operator is

$$\mathbf{C_d}^{ep} = (\mathbf{I} - \mathbf{D}) \cdot \mathbf{C}^{ep} \tag{6}$$

which is founded in the effective interface stress space (see Section 4).

3. Plasticity-based interface model

The constitutive interface model is now reformulated in terms of the incremental effective normal ($\widetilde{\sigma}_N$) and shear ($\widetilde{\sigma}_T$) stresses, related to the dual in-plane ($\dot{u}$) and out-of-plane ($\dot{v}$) relative velocities.

3.1. Yielding/failure surface

The yield and maximum (failure) criteria are defined by means of the following three-parameter surface (outlining the hyperbola represented in Fig. 1)

$$f = \widetilde{\sigma}_T^2 - (c - \widetilde{\sigma}_N \tan\phi)^2 + (c - \chi \tan\phi)^2 \tag{7}$$

where the tensile strength χ (vertex of the hyperbola), the cohesion c and the frictional angle ϕ are internal parameters defining the evolution of the interface strength surface under mechanical loading.

It is worth mentioning that Eq. (7) outlines two main failure modes:

- *Mode I*: direct tensile fracture, which is obtained when the stress state reaches the intersection between the strength surface and the normal effective stress axis (i.e., the horizontal axis).
- *Mode II*: direct shear fracture under effective confinement. This failure mode is reached when the stress state reaches the asymptotic zone of the maximum strength surface of the interface.

3.2. Plastic flow rule

The vector of relative plastic displacement rates, according to a non-associated flow rule, can be defined as

$$\dot{\mathbf{u}}^{cr} = \dot{\lambda}\mathbf{m} \tag{8}$$

where λ is the non-negative plastic multiplier which derives from the classical Kuhn-Tucker loading/unloading and consistency conditions

Fig. 1. Failure hyperbola by [48], Mohr-Coulomb surface, plastic potential and modified flow rule.

$$\dot{\lambda} \geqslant 0, \quad f \leqslant 0, \quad \dot{\lambda}f = 0 \quad \text{Kuhn} - \text{Tucker}$$
$$\dot{f} = 0 \quad \text{Consistency} \tag{9}$$

where $f = f\left[\widetilde{\sigma}_N, \widetilde{\sigma}_T\right]$ is the yield condition of the interface while $\mathbf{m}$ the vector controlling the direction of the fracture displacements by means of a non-associated flow rule

$$\mathbf{m} = \mathbf{A} \cdot \mathbf{n} \tag{10}$$

being

$$\mathbf{n} = \frac{\partial f}{\partial \widetilde{\mathbf{t}}} = \left[\frac{\partial f}{\partial \widetilde{\sigma}_N}, \frac{\partial f}{\partial \widetilde{\sigma}_T}\right]^t = \left[2\tan\phi(c - \widetilde{\sigma}_N \tan\phi), 2\widetilde{\sigma}_T\right]^t \tag{11}$$

the direction of the associated plastic flow.

The transformation matrix $\mathbf{A}$ in Eq. (10) is

$$\mathbf{A} = \begin{cases} \begin{pmatrix} \frac{\tan\beta}{\tan\phi} & 0 \\ 0 & 1 \end{pmatrix} & \text{if } \widetilde{\sigma}_N \geqslant 0 \\ \begin{pmatrix} \left[1 - \frac{|\widetilde{\sigma}_N|}{\widetilde{\sigma}_{dil}}\right]\frac{\tan\beta}{\tan\phi} & 0 \\ 0 & 1 \end{pmatrix} & \text{if } -\widetilde{\sigma}_{dil} \leqslant \widetilde{\sigma}_N < 0 \\ \begin{pmatrix} 0 & 0 \\ 0 & 1 \end{pmatrix} & \text{if } \widetilde{\sigma}_N < -\widetilde{\sigma}_{dil} \end{cases} \tag{12}$$

where $\tan\beta$ is the dilation angle of the plastic potential (Fig. 1): with $0 \leqslant \tan\beta \leqslant \tan\phi$. Thereby, the parameter $\widetilde{\sigma}_{dil}$ represents the normal effective stress at which the dilatancy vanishes [38].

3.3. Softening/re-hydration evolution law

In this proposal a multiplicative decomposition is considered for the internal variables controlling the evolution of the interface yield surface in post-peak regime. This decomposition involves two components describing the post-peak response due to the mechanical and the hydraulic effects, as

$$p_i = g_1\left(S[\xi_{p_i}]\right) g_2\left(\text{SH}[\psi]\right) p_{0i} \tag{13}$$

where p_i alternatively represents χ, c and $\tan\phi$ of Eq. (7) while ξ_{p_i} accounts for the effect of the ratio between the spent fracture work against the available energies (in mode I or II) and ψ is the self-healing porosity factor.

Eq. (13) defines the typical evolution law of the internal parameters from their maximum (or initial) values, $p_i = p_{0i}$, to the residual ones. In this sense, the following scaling functions are proposed for taking into account fracture processes caused by mechanical effects

$$g_1\left(S[\xi_{p_i}]\right) = \left(1 - \left(1 - r_{p_i}\right)S[\xi_{p_i}]\right), \tag{14}$$

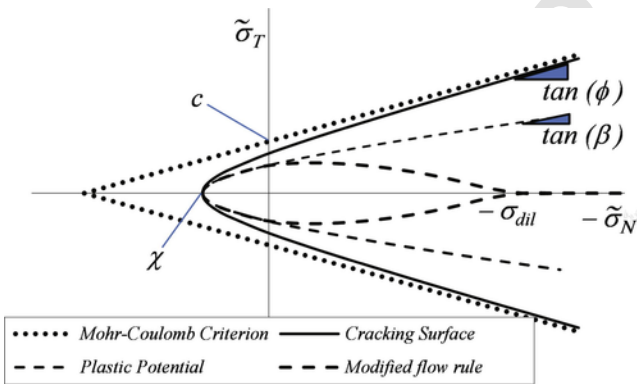and the restoration of internal proprieties due to self-healing

$$g_2\left(\mathrm{SH}[\psi]\right) = \left(\mathrm{SH}[\psi]\right) sh, \tag{15}$$

where r_{pi} measures the residual amounts of the internal parameters under mechanical loadings while *sh* a self-healing scalar parameter.

3.3.1. Softening due to mechanical fracture

The scaling function $S[\xi_{p_i}]$ in Eqs. (13) and (14) is defined by means of the following relationship

$$S[\xi_{p_i}] = \frac{e^{-\alpha_{p_i}\xi_{p_i}}}{1 + (e^{-\alpha_{p_i}} - 1)\xi_{p_i}} \tag{16}$$

whereby the parameter α_{p_i} controls the decay form of the internal parameter, while the non-dimensional variable ξ_{p_i} accounts for the influence on $S[\xi_{p_i}]$ of the ratio between the fracture work (currently spent) and the available fracture energy in mode I or II (G_f^I or G_f^{IIa}) according to the following C^1 continuity function proposed by [39]

$$\xi_\chi = \begin{cases} \frac{1}{2}\left[1 - \cos\left(\frac{\pi W_{cr}}{G_f^I}\right)\right] & \text{if } W_{cr} \leqslant G_f^I, \\ 1 & \text{otherwise} \end{cases} \tag{17}$$

$$\begin{aligned} \xi_c &= \xi_{\tan\phi} \\ &= \begin{cases} \frac{1}{2}\left[1 - \cos\left(\frac{\pi W_{cr}}{G_f^{IIa}}\right)\right] & \text{if } W_{cr} \leqslant G_f^{IIa}. \\ 1 & \text{otherwise} \end{cases} \end{aligned} \tag{18}$$

The fracture work spent, W_{cr}, spent during an opening-sliding process, controls the evolutions of the material parameters χ, c and $\tan\phi$ in softening regime of the interface response. Particularly, the variable W_{cr} defines the necessary amount of released energy to open a single crack in tensile and/or shear fracture mode due to normal $\tilde{\sigma}_N$ and/or tangential $\tilde{\sigma}_T$ effective stresses.

Therefore, the rate of the fracture work $\dot{W}_{cr}$ spent, during a generic fracture process, is defined as follows

$$\begin{aligned} \dot{W}_{cr} &= \tilde{\sigma}_N \cdot \dot{u}^{cr} + \tilde{\sigma}_T \cdot \dot{v}^{cr}, \quad \text{if } \tilde{\sigma}_N \geqslant 0, \\ \dot{W}_{cr} &= \left[\tilde{\sigma}_T - |\tilde{\sigma}_N|\tan(\phi)\right] \cdot \dot{v}^{cr}, \quad \text{if } \tilde{\sigma}_N < 0. \end{aligned} \tag{19}$$

Finally, the total dissipated work is obtained by integrating the fracture work increments during the entire fracture process.

3.3.2. Softening due to self-healing porosity

The $g_2\left(\mathrm{SH}[\psi]\right)$ function in Eq. (13) describes the post-peak response of the interface due to the self-healing phenomenon through the so-called self-healing porosity. This parameter defines the evolution of the concrete open-porosity during self-healing processes as outlined in Eq. (15), being

$$\mathrm{SH}[\psi] = \frac{e^{-\varsigma_{p_i}\psi}}{1 + (e^{-\varsigma_{p_i}} - 1)\psi} \tag{20}$$

where ς_{p_i} controls the decay forms of the porosity-based post-peak function $\mathrm{SH}[\psi]$ (Fig. 2), while ψ is the self-healing porosity factor which is defined as follows

$$\psi = \frac{\phi_c - \phi_f}{\phi_0 - \phi_f} \quad \phi_c \in \left[\phi_0, \phi_f\right] \tag{21}$$

being ϕ_c the current open porosity of the interface plane which varies during the re-hydration and self-healing process from its initial value ϕ_0 up to the maximum or final one ϕ_f.

4. Isotropic damage formulation

In this study, a scalar-type approach is employed to describe the isotropic damage as proposed through Eqs. (4)–(6).

Relevant researches on this topic assumed an exponential form of the damage variable as function of the equivalent plastic tensile strain [40–43]. In this interface model proposal two independent scalar damages are considered, d^I and d^{IIa}, which vary into the range [0,1]. Thereby, $d^{I/IIa} = 0$ corresponds to the undamaged interface, while $d^{I/IIa} = 1$ to the fully damaged one.

The damage evolution is described by means of the following unified rule based on the fracture work [44]

$$d^{I/IIa} = \frac{e^{-\beta_d}\left(\frac{W_{cr}}{G_f^{I/IIa}}\right)^{\alpha_d}}{1 + (e^{-\beta_d} - 1)\left(\frac{W_{cr}}{G_f^{I/IIa}}\right)^{\alpha_d}} \tag{22}$$

whereby the parameters $\alpha_d \geqslant 0$ and β_d control the decay form of the damage induced by fracture, as shown in Figs. 3 and 4.
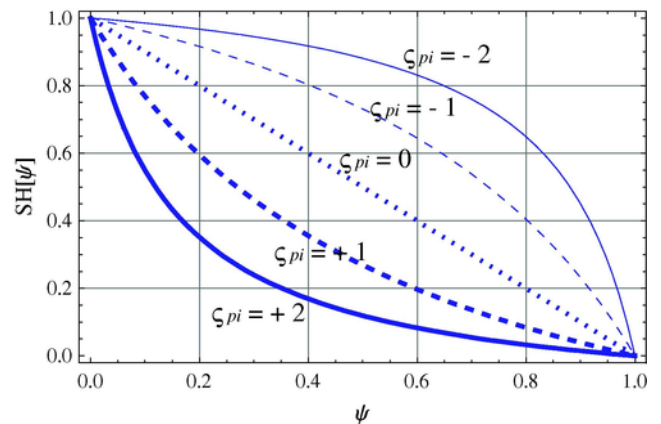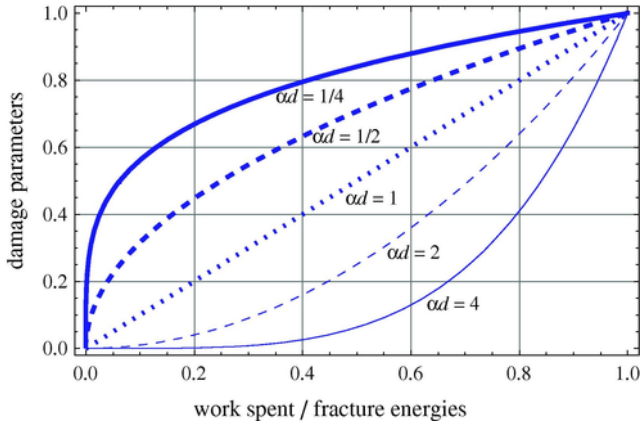

Fig. 2. Porosity-based function $\mathrm{SH}[\psi]$.

Fig. 3. $d^{I/IIa}$ vs. $\frac{W_{cr}}{G_f^{I/IIa}}$ damage function for several values of α_d, keeping $\beta_d = 0$.
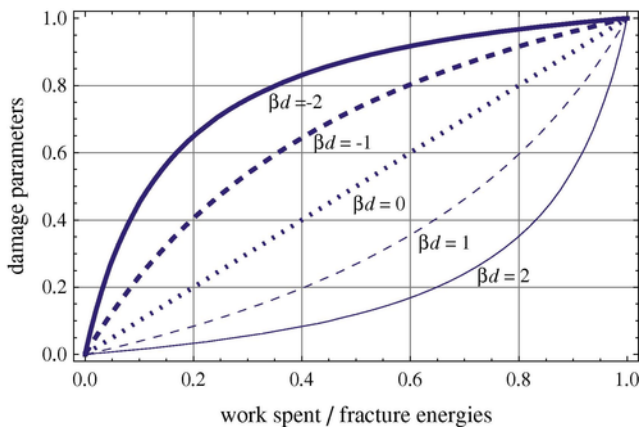

Fig. 4. $d^{I/IIa}$ vs. $\frac{W_{cr}}{G_f^{I/IIa}}$ damage function for several values of β_d, keeping $\alpha_d = 1$.

Finally, Eq. (4) expands into

$$\mathbf{C_d} = \begin{pmatrix} 1 - d^I & 0 \\ 0 & 1 - d^{IIa} \end{pmatrix} \cdot \begin{pmatrix} k_N & 0 \\ 0 & k_T \end{pmatrix} \tag{23}$$

while the tangential elastic-damage-plastic operator of Eq. (6) can be written as

$$\mathbf{C_d}^{ep} = \begin{pmatrix} 1 - d^I & 0 \\ 0 & 1 - d^{IIa} \end{pmatrix} \cdot \left(\mathbf{C} - \frac{\mathbf{C} \cdot \mathbf{m} \otimes \mathbf{n} \cdot \mathbf{C}}{H + \mathbf{n} \cdot \mathbf{C} \cdot \mathbf{m}} \right) \tag{24}$$

being H the so-called softening parameter [20].

5. Outline of the experimental test results

The composition of the investigated concrete mixtures is listed in Table 1. Both autogenous healing and engineered one, through the use of crystalline admixtures, have been studied.

The employed crystalline admixture consists of a blend of cement, sand and microsilica; SEM magnified particles are shown in Figs. 5a-b: they have irregular shape and size in the range of about 1–20 μm and their morphology is similar to that of cement grains. EDS analysis confirmed the presence of calcium, oxygen, silicon, magnesium, alu-

Table 1
Mix design of investigated cement-based materials.

Constituents	Dosage (kg/m³)	
	Ref.	Ref.
Cement CEM II 42.5 A/L	300	300
Crystalline admixture	=	3
Water	180	180
	w/c = 0.6	
Superplasticizer	3	3
NW fine aggregate 0–4 mm	1080	1077
NW coarse aggregate 4–16 mm	880	880

minum and potassium (Fig. 5c), once again comparably to ordinary Portland cement, except for the slightly higher sulfur peak.

A three-stage dedicated experimental methodology has been developed for the characterization of self-healing through the quantification of its effects on the recovery of mechanical properties:

- Pre-cracking the specimens, up to crack-opening thresholds, under 3-point-bending test schemes; geometry of the specimens and pre-cracking thresholds, were tailored to the material. Geometry of specimens and test set-ups are shown in Fig. 6.
- Exposing the specimens to different environments and for different times.
- Testing the specimens, after conditioning, up to failure according to the same set-up employed for the pre-cracking.

More specifically, several concrete slabs (1000 mm long × 500 mm wide × 50 mm thick) were cast with and without additives. After three days curing in fog room at 20 °C temperature, 95% Relative Humidity (RH) and under wet towels, such slabs were cut into 500 mm × 100 mm × 50 mm prismatic specimens (Fig. 6a). Beam specimens were then cured in the same fog room for a time period between 35 and 42 days. In order to evaluate the concrete self-healing capacity and its effect on the recovery of mechanical properties, after the aforementioned curing period, the beam specimens were pre-cracked up to the residual crack opening of 250 μm. The three-point beam test (3 PB) set-up outlined in Fig. 6b was followed using the Crack Opening Displacement (COD) at mid-span as a control variable. All the specimens were then subjected to different controlled exposure conditions: (i) immersion in water at constant temperature, equal to 20 °C, or (ii) exposure to air (while daily recording minimum and maximum temperature and average RH [7]). Four times of exposure were considered for both under-water and air conditioning: i.e., 1, 2, 6 and 12 months. Finally, at the end of the scheduled exposure times, the 3pb tests were performed again, on each specimen, until its complete failure.

Table 2 provides a synopsis of the experimental program as a whole. Comparative analysis of pre-cracking and post-conditioning experimental results, in terms of nominal bending stress vs. COD curves, allows to assess the recovery of residual strength, stiffness and, in case, ductility, as a proof of the occurred crack healing, complemented by optical microscopy observation of the partially or even totally sealed cracks.

In Figs. 7–10, experimental results in terms of vertical load vs. COD curves are shown. Images of healed cracks (highlighted in Fig. 11) support the aforementioned statements. Moreover, pictures from SEM analysis (see Fig. 12) highlight on crack surfaces the presence healing products on crack surfaces, whose composition resembles that of cement hydration products and is coherent with the one of the additive employed as a self-healing catalyst.

It is worth mentioning that for the sake of brevity the complete description and discussion of the experimental programme is omitted
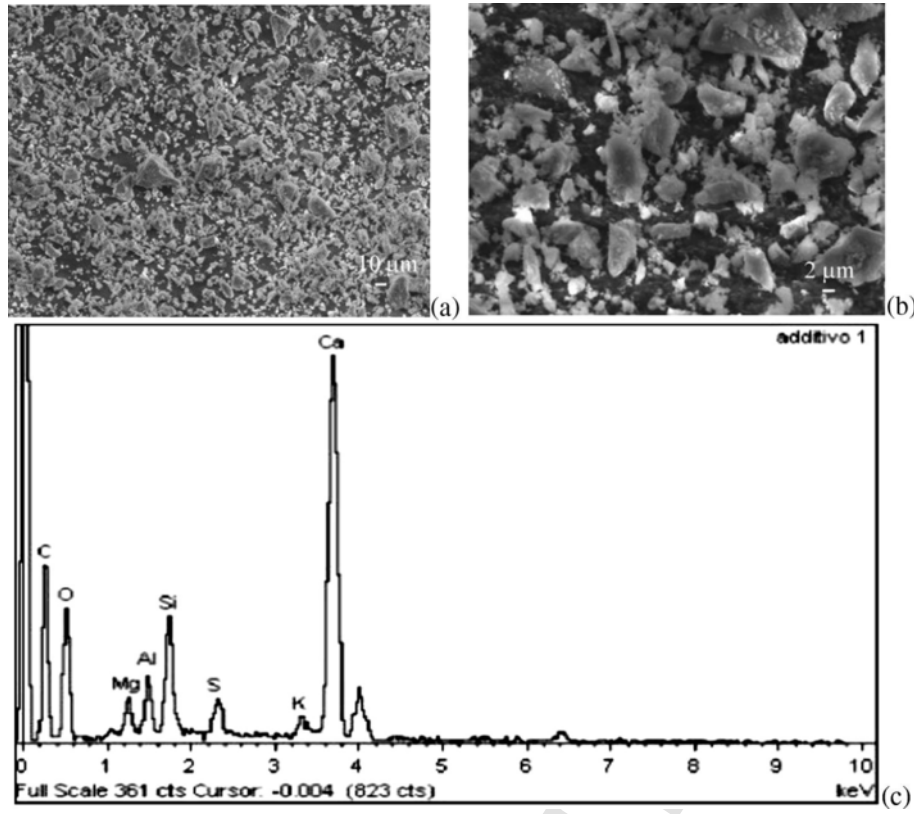
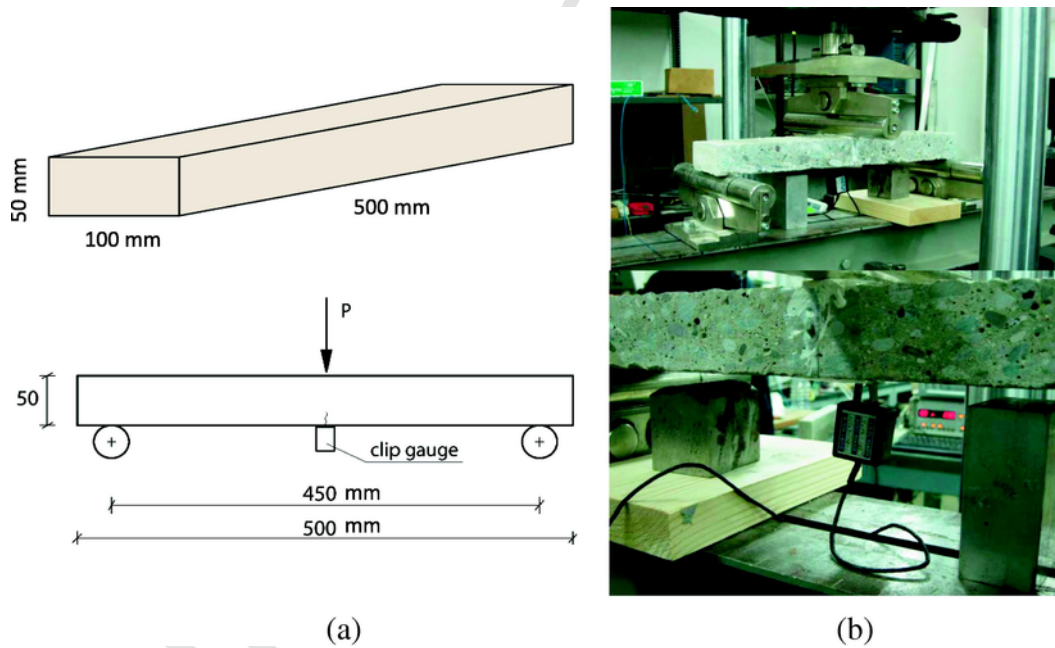**Fig. 5.** SEM magnification (a and b) and EDS analysis (c) of admixture particles.

Fig. 6. Concrete pre-cracking and post-conditioning testing: (a) geometric details and (b) schematic test setup.

Table 2
Experimental programme synopsis.

	Concrete with crystalline admixture	Concrete without crystalline admixture
Crack opening	250 μm	
Exposure condition	Time (months)	
Water immersion	1, 2, 6 and 12	
Air exposure	1, 2, 6 and 12	

in this work. However deep and detailed information about it are available in the paper published by two of the Authors (see [7]).

6. Validation of the model and numerical predictions

This section aims at validating the proposed interface model by performing and comparing numerical examples against the experimental results outlined in the previous section.

The numerical results try to simulate the specimens tested under three-point bending. Particularly, in order to evaluate the self-healing capacity of concrete at numerical standpoint and its effects on the recovery of the mechanical properties, three numerical steps were considered into the FEM analyses: (i) in the first one, the beam specimen was pre-cracked up to a certain level of COD (namely residual crack opening); (ii) the second step which is characterized by a considered elapsed time (exposure time) and finally (iii) the ultimate step which

allows to evaluate the total failure of the specimen and with which it can be evaluate the self-healing capacity of concrete.

For the calibration purpose of the numerical examples, four families (having different exposure and/or mixture types of concrete) were considered as follows:

- AEWA: Air Exposure Without crystalline Admixture.
- AECA: Air Exposure with Crystalline Admixture.
- WEWA: Water Conditioning Without crystalline Admixture.
- WECA: Water Conditioning with Crystalline Admixture.

Finite element analyses adopt the geometry shown in Fig. 13 considering $100 \times 50 \times 450$ mm^3 concrete specimens according to [7]. Fig. 14 proposes the FE discretization employed in the present analysis. Plane stress hypothesis and displacement-based control are assumed. Four-node iso-parametric elements, equipped with a linear elastic model, have been adopted in the FE mesh, while all non-linearities are concentrated within zero-thickness interfaces defined throughout the adjacent edges of the finite elements in the cracked zone of the beam (Fig. 14). Particularly, non-linear porosity and fracture/damage-based interface rules were introduced in those interface elements according to the formulation outlined in Sections 2–4.

The key geometric and material properties of the numerical examples were chosen according to the experimental evidences [7]. Based on the calibration procedure, the elastic modulus and Poisson's ratio of concrete (continuous FEs) was $E_c = 21.70$ GPa and $\nu = 0.17$ for all mixtures, respectively. Then, the mechanical parameters of the interface model are here listed: $k_N = 500$ MPa/mm, $k_T = 200$ MPa/mm

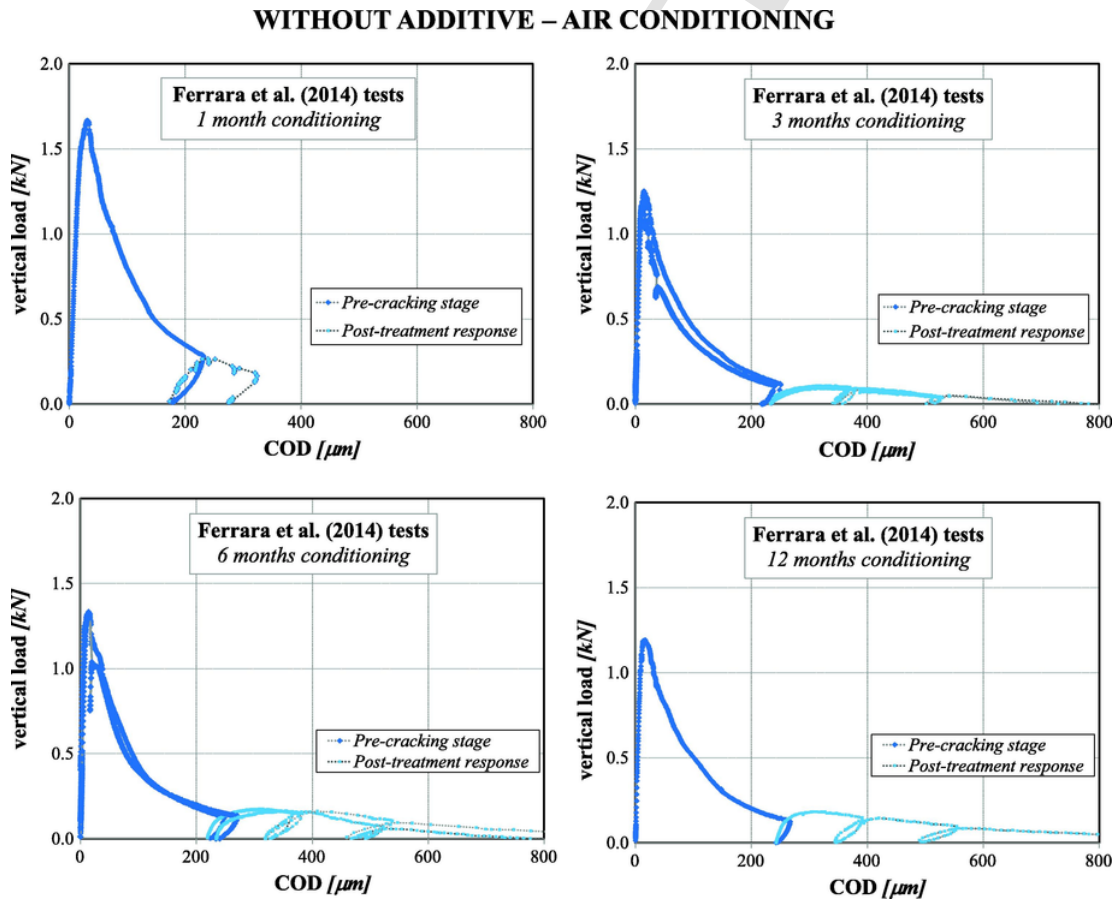## WITHOUT ADDITIVE – AIR CONDITIONING

Fig. 7. Experimental load-deflection behavior: specimens under air exposure without crystalline admixtures [7].
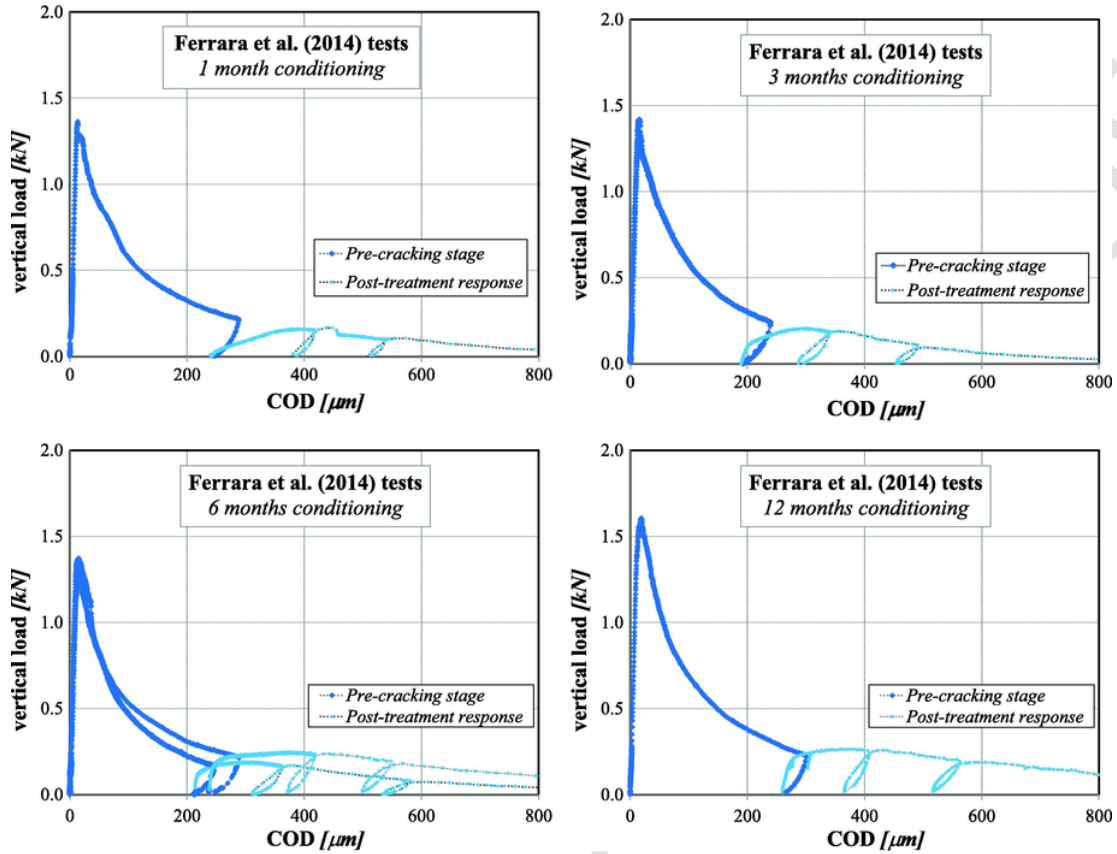
WITH ADDITIVE – AIR CONDITIONING

Fig. 8. Experimental load-deflection behavior: specimens under air exposure with crystalline admixtures [7].

, $\tan\phi_0 = 0.6$, $\tan\beta = 0.3$, $r_{\tan\phi} = 0.67$, $\sigma_{dil} = 10$ MPa, for all mixtures. Finally, Table 3 figures out the calibrated parameters for the fracture-based, self-healing and damage functions of the interface model.

Notice that as a result of the calibration procedure, ξ_{p_i} is negative in every considered test and conditioning case. This is actually expected as it is related to the reduction of the rate of hydration (or re-hydration) under increasing exposure/conditioning time frame. As a matter of fact, high values of ψ mainly represent small exposure/conditioning time frame (and vice versa small ψ values account for elevated exposure/conditioning time frames). This behavior, which always occurs in all hydration process of cementitious materials [45–47], takes place also in re-hydration self-healing phenomena.

After the calibration procedure, Figs. 15–18(a) show the force-deflection curves against the corresponding experimental results. All those tests refer to 12-months conditioning type. It can be observed that the post-cracking response is very well captured through the considered discontinuous approach based on non-linear interfaces. Furthermore, the comparison between the experimental and numerical results in terms of the load vs. crack opening displacement (COD) highlights as the model is able to predict both the softening behavior in the pre-cracking stage and the self-healing recovery of the load bearing capacity after the conditioning with respect to the unloading value at which the value decayed in the pre-cracking stage.

On the other hand, Figs. 15–18(b) reproduce the comparisons in terms of a proposed "Index of load Recovery" (*IR*) between the numerical simulations against the experimental data for all conditioning types and times for both (with and without crystalline admixtures)

the analyzed mixtures. IR was defined as follows:

$$IR = \frac{f_{R,\max\,POST-CONDITIONING} - f_{R,unloading\;PRE-CRACK}}{f_L} \quad (25)$$

where $f_L = \frac{3P_L l}{2bh^2}$, being P_L the maximum flexural load; b, h and l are the width, height and length of the beam, respectively. $f_{R,\max\,POST-CONDITIONING}$ and $f_{R,unloading\,PRE-CRACK}$ represent the post-cracking flexural stresses (evaluated similarly to f_L) related to the $P_{R,\max\,POST-CONDITIONING}$ and $P_{R,unloading\,PRE-CRACK}$ loads, respectively. Moreover, $P_{R,\max\,POST-CONDITIONING}$ represents the flexural load corresponding to the maximum COD value of the pre-cracking stage while $P_{R,unloading\,PRE-CRACK}$ is the maximum flexural load of the post-treatment stage.

Finally, the recovery predictions of the flexural loads are well reproduced by means of the numerical model as indicated throughout Figs. 15–18(b), especially for the cases of water conditioning where the scatter of the experimental results is less pronounced.

7. Conclusions

This paper addressed the formulation of a fracture/damage and porosity-based interface model for analyzing post-peak behavior of cementitious composites due to the combined action of mechanical loading and self-healing phenomenon. The model is calibrated with ex-
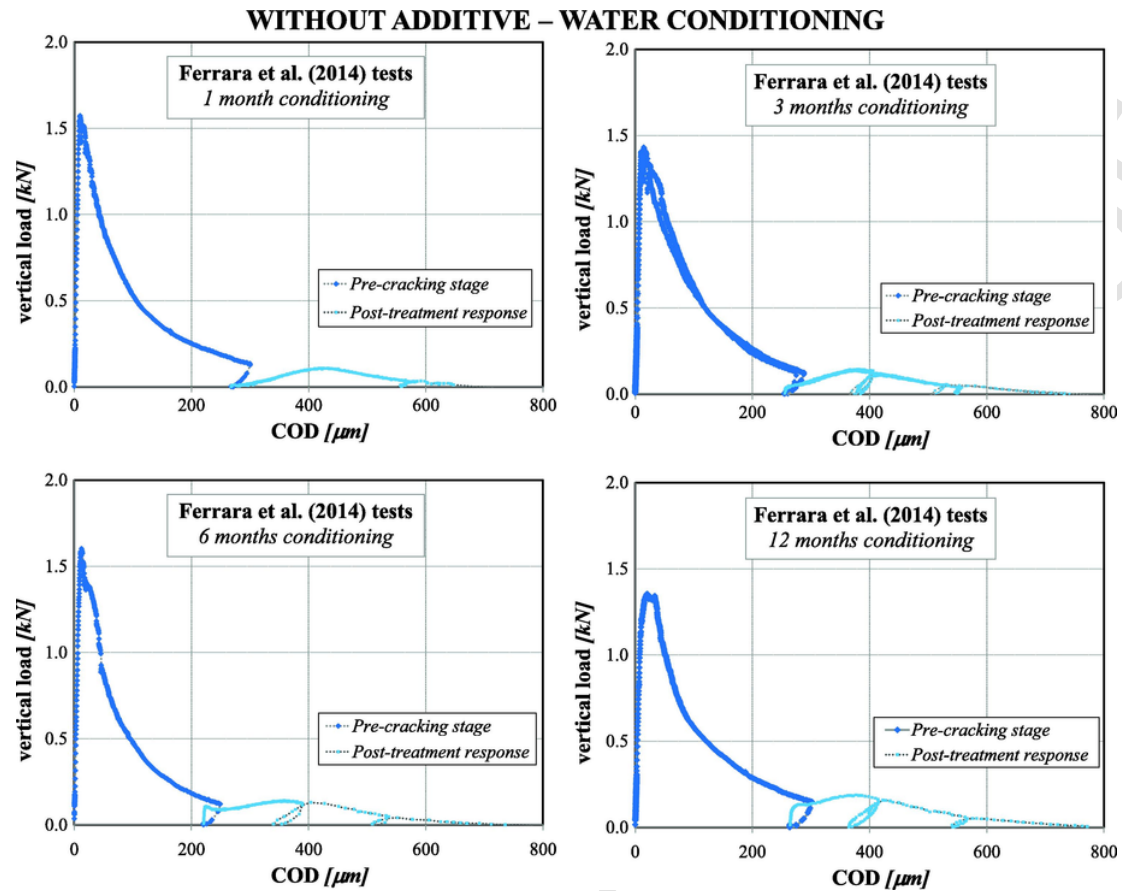
Fig. 9. Experimental load-deflection behavior: specimens conditioned under water without crystalline admixtures [7].

perimental results involving self-healing processes and, then, the predictive capabilities of the interface formulation is evaluated with further experimental test results.

Based on the features of the proposed interface model and the obtained results, following conclusions can be drawn out:

- The proposed formulation explicitly model the porosity evolutions due to self-healing.
- Novel concept and formulations were introduced to account for pore closure and evolution due to self-healing phenomenon, and to describe the resulting evolution of concrete post-peak strength.
- Numerical analyses demonstrated the predictive capabilities of the constitutive model in terms of the most relevant aspects of the mechanical behavior of concrete after crack closure due to self-healing processes and under consideration of several exposure conditions and different concrete mixtures.

Further developments are currently ongoing for better understanding other relevant aspects, such as the prediction and modeling of the moisture diffusion in concrete which could directly influence the re-hydration effect of cementitious materials. As a matter of fact, several parameters based on physical arguments which are involved in the proposed formulation such as porosity variables, self-healing products and re-hydration phenomena could be directly related to diffusion and reaction processes and still require more investigations. As a matter of principle, this is a straightforward evolution of the model presented in this paper which was only limited to the study of the

mechanical and fracture mechanisms effects due self-healing phenomena.

Finally, it is nowadays widely accepted that complex multiphysical processes in composite materials like concrete such as self-healing effects may be more accurately modeled through multiscale analyzes based on homogenization procedures as well as through full 3D formulations. The interface model proposed in this paper can be certainly employed in multiscale studies whereby some of the involved physical or kinematic variables could be evaluated through homogenization procedures. Also, the proposed interface model for self-healing processes in concrete can be extended for 3D analysis and computational simulations. Precisely, the extension to a 3D interface model formulation represents a very interesting item for future researches associated to self-healing computational modeling.

Acknowledgments
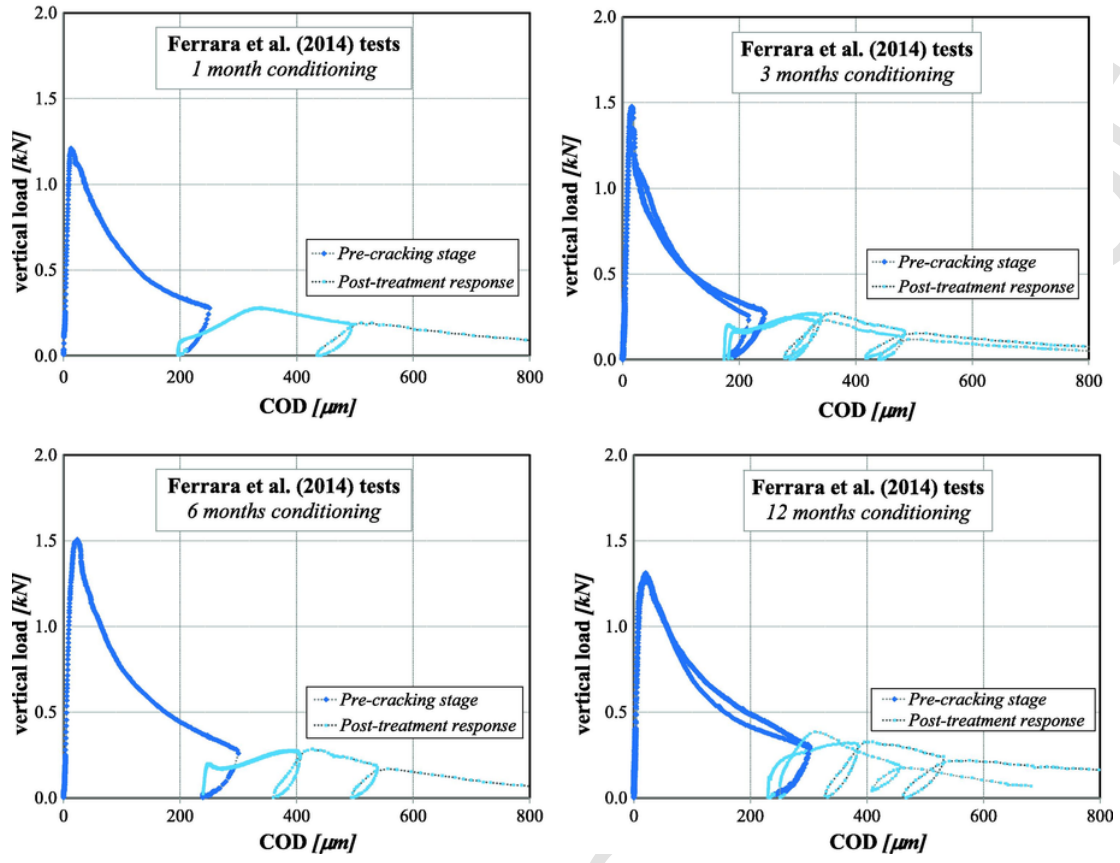
WITH ADDITIVE – WATER CONDITIONING

Fig. 10. Experimental load-deflection behavior: specimens conditioned under water with crystalline admixtures [7].
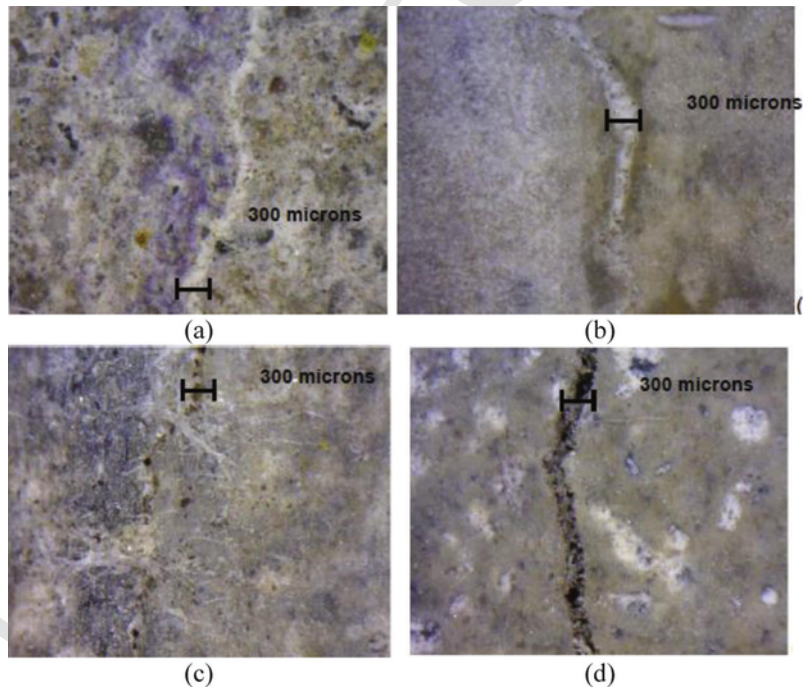

Fig. 11. Healed/healing cracks for specimens with (a and c) and without (b and d) crystalline additive after six months of immersion in water (a and b) and exposure to air (c and d).
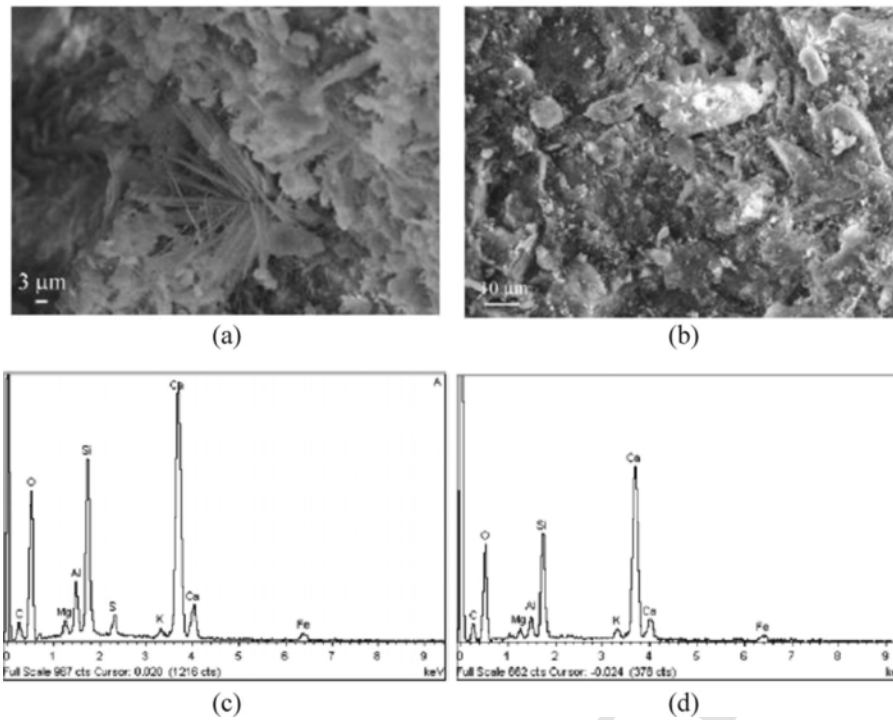
Fig. 12. SEM images and EDS analyses for specimens with (a and c) and without (b and d) crystalline additive after six months of immersion in water.
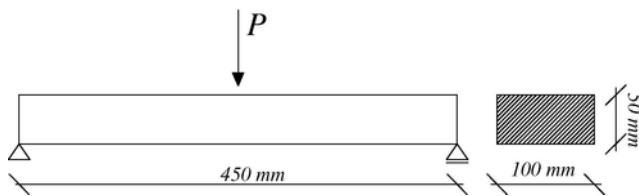

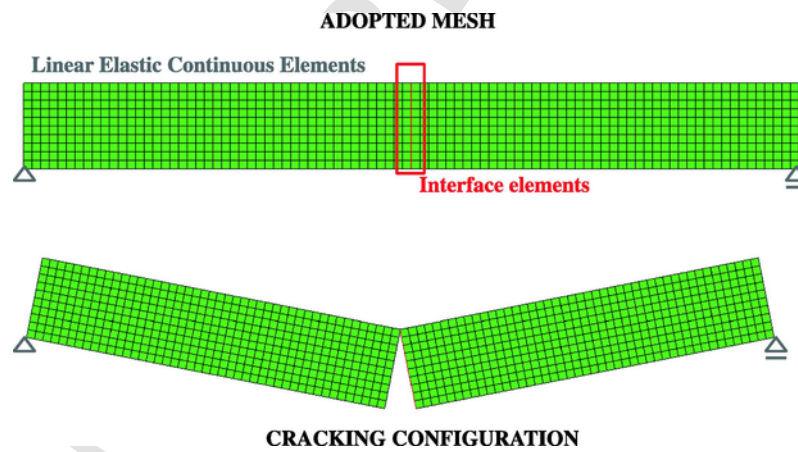**Fig. 13.** Specimen geometry according to experimental tests on 3 PB [7].

Fig. 14. Finite element mesh, interfaces and possible crack path of the three-point bending.

Table 3
Fracture-based, self-healing and damage parameters employed in the numerical analyses.

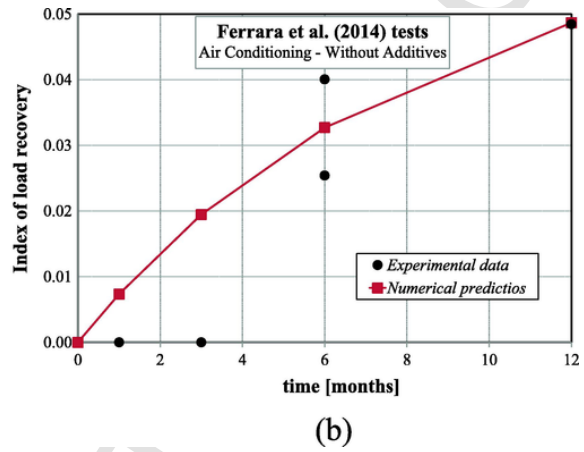| Test label	Fracture-based interface				Porosity-based scaling rule			Damage parameters	
	c_o (MPa)	c_o (MPa)	G_f^l (N/mm)	G_f^{IIa} (N/mm)	α_c	ζ_{pi}	sh (%)	α_d	β_d
AEWA	1.90	4.20	0.10	1.00	0.25	−0.73	7.24	4.0	−4.0
AECA	2.96	6.37	0.17	1.70	1.00	−0.85	4.94	4.0	−3.5
WEWA	2.18	4.69	0.13	1.30	1.00	−0.04	5.07	4.0	−4.0
WECA	1.95	4.20	0.18	1.80	1.00	−1.50	5.79	4.0	−4.0

(a)   (b)

Fig. 15. 3 PB load-deflection response: "AEWA" experimental results [7] vs. numerical predictions.
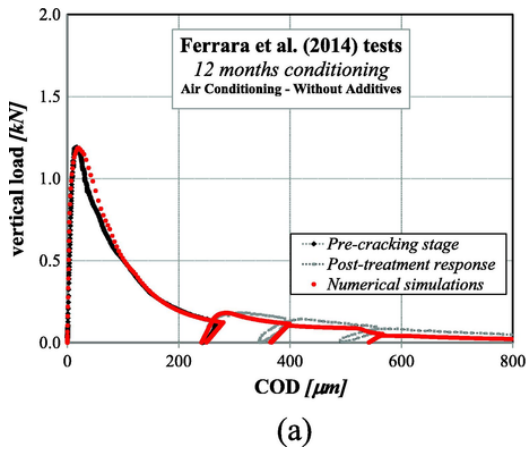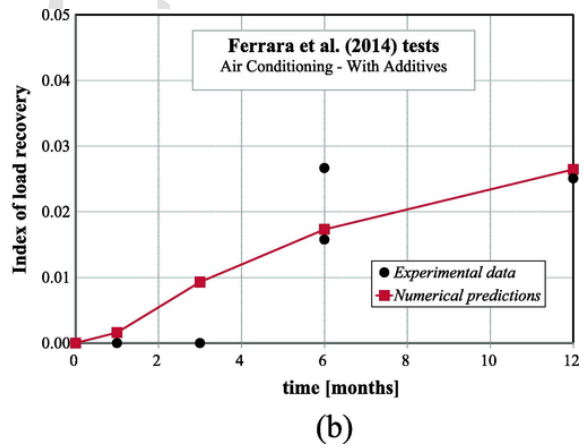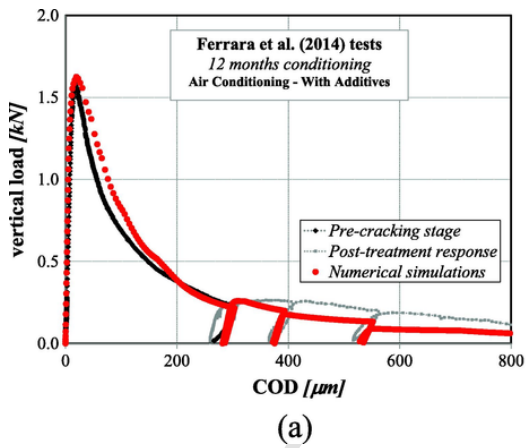

(a)   (b)

Fig. 16. 3 PB load-deflection response: "AEWA" experimental results [7] vs. numerical predictions.

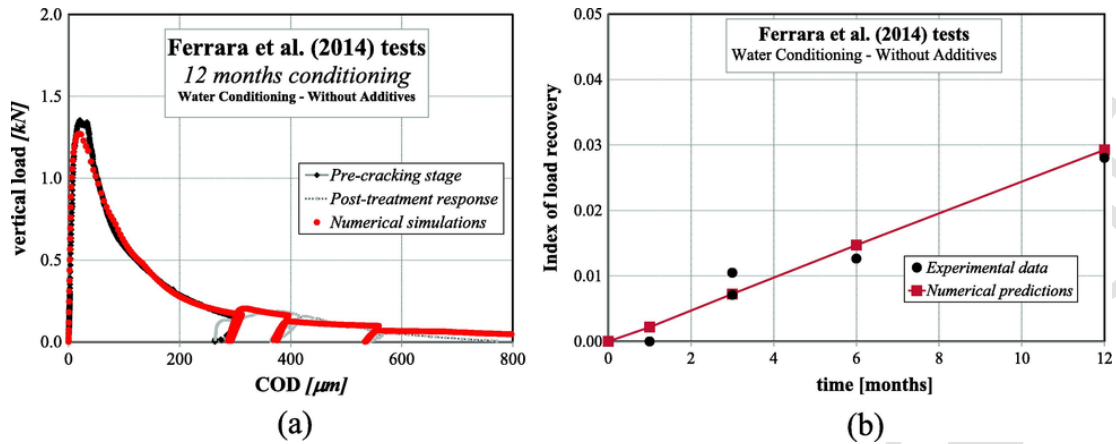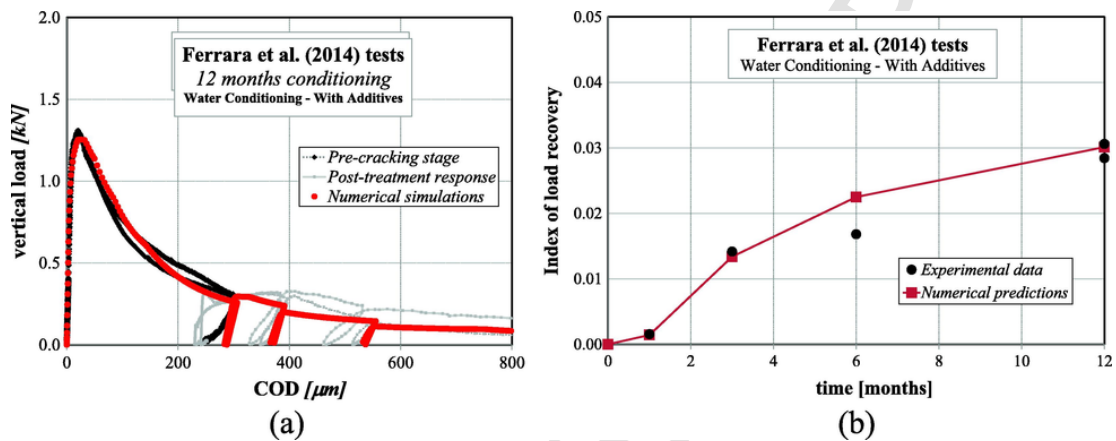**Fig. 17.** 3 PB load-deflection response: "WEWA" experimental results [7] vs. numerical predictions.

Fig. 18. 3 PB load-deflection response: "WECA" experimental results [7] vs. numerical predictions.

References

[1] R. Rehan, M. Nehdi, Carbon dioxide emissions and climate change: policy implications for the cement industry, Environ Sci Pol 8 (2005) 105–114.

[2] C. Lima, A. Caggiano, C. Faella, E. Martinelli, M. Pepe, R. Realfonzo, Physical properties and mechanical behaviour of concrete made with recycled aggregates and fly ash, Construct Build Mater 47 (2013) 547–559.

[3] H.M. Jonkers, A. Thijssen, G. Muyzer, O. Copuroglu, E. Schlangen, Application of bacteria as self-healing agent for the development of sustainable concrete, Ecol Eng 36 (2010) 230–235.

[4] M.S. Vekariya, J. Pitroda, Bacterial concrete: new era for construction industry, Int J Eng Trends Technol 4 (2013) 4128–4137.

[5] De Rooij M, Schlangen E. Self-healing phenomena in cement-based materials. Draft of State-of-the-Art report of RILEM Technical Committee; 2011.

[6] K. Sisomphon, O. Copuroglu, E. Koenders, Self-healing of surface cracks in mortars with expansive additive and crystalline additive, Cem Concr Compos 34 (2012) 566–574.

[7] L. Ferrara, V. Krelani, M. Carsana, A fracture testing based approach to assess crack healing of concrete with and without crystalline admixtures, Construct Build Mater 68 (2014) 535–551.

[8] V. Wiktor, H.M. Jonkers, Quantification of crack-healing in novel bacteria-based self-healing concrete, Cem Concr Compos 33 (2011) 763–770.

[9] K.V. Tittelboom, E. Tsangouri, D.V. Hemelrijck, N.D. Belie, The efficiency of self-healing concrete using alternative manufacturing procedures and more realistic crack patterns, Cem Concr Compos 57 (2015) 142–152.

[10] H. Mihashi, T. Nishiwaki, Development of engineered self-healing and self-repairing concrete-state-of-the-art report, J Adv Concr Technol 10 (2012) 170–184.

[11] M. Wu, B. Johannesson, M. Geiker, A review: Self-healing in cementitious materials and engineered cementitious composite as a self-healing material, Construct Build Mater 28 (2012) 571–583.

[12] R.P. Wool, Self-healing materials: a review, Soft Matter 4 (2008) 400–418.

[13] E. Martinelli, E.A. Koenders, A. Caggiano, A numerical recipe for modelling hydration and heat flow in hardening concrete, Cem Concr Compos 40 (2013) 48–58.

[14] H. He, Z. Guo, P. Stroeven, M. Stroeven, L.J. Sluys, Self-healing capacity of concrete-computer simulation study of unhydrated cement structure, Image Anal Stereol 26 (2011) 137–143.

[15] H. Huang, G. Ye, Simulation of self-healing by further hydration in cementitious materials, Cem Concr Compos 34 (2012) 460–467.

[16] Z. Lv, H. Chen, Modeling of self-healing efficiency for cracks due to unhydrated cement nuclei in hardened cement paste, Proc Eng 27 (2012) 281–290.

[17] B. Hilloulin, F. Grondin, M. Matallah, A. Loukili, Modelling of autogenous healing in ultra high performance concrete, Cem Concr Res 61–62 (2014) 64–70.

[18] G. Di Luzio, G. Cusatis, Solidification-microprestress-microplane (SMM) theory for concrete at early age: theory, validation and application, Int J Solids Struct 50 (2013) 957–975.

[19] Di Luzio G, Ferrara L, Krelani V. A numerical model for the self-healing capacity of cementitious composites. In: Proceedings of EURO-C 2014, vol. 2. p. 741–7.

[20] A. Caggiano, G. Etse, Coupled thermo-mechanical interface model for concrete failure analysis under high temperature, Comp Meth Appl Mech Eng 289 (2015) 498–516.

[21] M.A.H. Ardebili, S.M.S. Kolbadi, M. Heshmati, H. Mirzabozorg, Nonlinear analysis of concrete structural components using co-axial rotating smeared crack model, J Appl Sci 12 (2012) 221.

[22] P. Folino, G. Etse, Performance dependent model for normal and high strength concretes, Int J Solids Struct 49 (2012) 701–719.

[23] G. Etse, K. Willam, Fracture energy formulation for inelastic behavior of plain concrete, J Eng Mech 120 (1994) 1983–2011.

[24] M. Ripani, G. Etse, S. Vrech, J. Mroginski, Thermodynamic gradient-based poroplastic theory for concrete under high temperatures, Int J Plast 61 (2014) 157–177.

[25] Y. Mi, M. Crisfield, G. Davies, H. Hellweg, Progressive delamination using interface elements, J Compos Mater 32 (1998) 1246–1272.

[26] I. Carol, C.M. López, O. Roa, Micromechanical analysis of quasi-brittle materials using fracture-based interface elements, Int J Numer Meth Eng 52 (2001) 193–215.

[27] G. Cusatis, Z.P. Bazant, L. Cedolin, Confinement-shear lattice model for concrete damage in tension and compression: II. Computation and validation, J Eng Mech 129 (2003) 1449–1458.

[28] E. Schlangen, E. Garboczi, Fracture simulations of concrete using lattice models: computational aspects, Eng Fract Mech 57 (1997) 319–332.

[29] P. Stroeven, H. He, Z. Guo, M. Stroeven, Particle packing in a model concrete at different levels of the microstructure: evidence of an intrinsic patchy nature, Mater Character 60 (2009) 1088–1092.

[30] M. Jirásek, Z.P. Bazant, Particle model for quasibrittle fracture and application to sea ice, J Eng Mech 121 (1995) 1016–1025.

[31] J. Oliver, A. Huespe, S. Blanco, D. Linero, Stability and robustness issues in numerical modeling of material failure with the strong discontinuity approach, Comp Meth Appl Mech Eng 195 (2006) 7093–7114.

[32] D. Linero, J. Oliver, A. Huespe, M. Pulido, Cracking modeling in reinforced concrete via the strong discontinuity approach, Comput Model Concr Struct, London (2006) 173–182.

[33] T. Elguedj, A. Gravouil, A. Combescure, Appropriate extended functions for X-FEM simulation of plastic fracture mechanics, Comp Meth Appl Mech Eng 195 (2006) 501–515.

[34] T. Hettich, A. Hund, E. Ramm, Modeling of failure in composites by X-FEM and level sets within a multiscale framework, Comp Meth Appl Mech Eng 197 (2008) 414–424.

[35] T. Belytschko, D. Organ, C. Gerlach, Element-free Galerkin methods for dynamic fracture in concrete, Comp Meth Appl Mech Eng 187 (2000) 385–399.

[36] T. Belytschko, Y. Lu, L. Gu, M. Tabbara, Element-free Galerkin methods for static and dynamic fracture, Int J Solids Struct 32 (1995) 2547–2570.

[37] J. Lemaitre, A continuous damage mechanics model for ductile fracture, J Eng Mater Technol 107 (1985) 83–89.

[38] A. Caggiano, G. Etse, E. Martinelli, Zero-thickness interface model formulation for failure behavior of fiber-reinforced cementitious composites, Comp Struct 98–99 (2012) 23–32.

[39] A. Caballero, K. Willam, I. Carol, Consistent tangent formulation for 3d interface modeling of cracking/fracture in quasi-brittle materials, Comp Meth Appl Mech Eng 197 (2008) 2804–2822.

[40] S. Yazdani, H. Schreyer, Combined plasticity and damage mechanics model for plain concrete, J Eng Mech (1990).

[41] J. Lee, G.L. Fenves, Plastic-damage model for cyclic loading of concrete structures, J Eng Mech 124 (1998) 892–900.

[42] J. Lubliner, J. Oliver, S. Oller, E. Onate, A plastic-damage model for concrete, Int J Solids Struct 25 (1989) 299–326.

[43] C. Koh, M. Teng, T. Wee, A plastic-damage model for lightweight concrete and normal weight concrete, Int J Concr Struct Mater 2 (2008) 123–136.

[44] L. Ferrara, M. di Prisco, Mode i fracture behavior in concrete: nonlocal damage modeling, J Eng Mech 127 (2001) 678–692.

[45] K. van Breugel, E. Koenders, Numerical simulation of hydration-driven moisture transport in bulk and interface paste in hardening concrete, Cem Concr Res 30 (2000) 1911–1914.

[46] E. Koenders, K. Van Breugel, Numerical modelling of autogenous shrinkage of hardening cement paste, Cem Concr Res 27 (1997) 1489–1499.

[47] E. Martinelli, E.A. Koenders, A. Caggiano, A numerical recipe for modelling hydration and heat flow in hardening concrete, Cem Concr Compos 40 (2013) 48–58.

[48] I. Carol, P. Prat, C. Lopez, Normal/shear cracking model: applications to discrete crack analysis, ASCE - J Eng Mech 123 (1997) 765–773.